Structure and local magnetic anisotropy of MBE-grown Co films

H. A. M. de Gronckel,* P. J. H. Bloemen, E. A. M. van Alphen, and W. J. M. de Jonge
Eindhoven University of Technology, Department of Physics, P.O. Box 513, 5600 MB Eindhoven, The Netherlands
(Received 20 December 1993)

Co films of 1000-Å thickness were grown by molecular-beam epitaxy on substrates of mica, oxidized silicon, and glass at temperatures between −33 °C and 800 °C. X-ray diffraction and nuclear magnetic resonance were used to study the structural quality and phase composition as a function of growth temperature and type of substrate. The magnetic anisotropy of the films was measured using vibrating-sample magnetometry. The film quality is observed to improve sharply for growth temperatures above 200 °C. Below this temperature the films have a strong polycrystalline character. Above this temperature the films on mica and oxidized silicon show well defined (111)/(00.2) texture and coherence lengths on the order of the film thickness. The structural phase composition depends on both substrate and growth temperature. For growth on mica at about 500 °C an almost single phased hcp Co film was obtained. Above this temperature the fcc phase dominates the structure, whereas below this temperature stacking faults dominate. For the films grown on oxidized silicon the structure is dominated by stacking faults and the fcc phase over the whole growth temperature range. The overall magnetic anisotropy of the films strongly depends on the structural phase composition. Its magnitude can be satisfactorily described by a compositional average of the respective bulk anisotropies.

I. INTRODUCTION

One of the interesting topics in the field of layered magnetic materials is the anisotropy. Due primarily to the fact that the magnetic anisotropy is composed of surface- and volume-related contributions, the resulting anisotropy of multilayered systems can be tailored by changing the volume-to-surface ratio. The most prominent example in this respect is the change in preferential direction of the magnetization for small layer thicknesses of the magnetic element from the commonly shape-induced in-plane orientation to the direction perpendicular to the plane.[1]

So far, the vast majority of experimental investigations has been focused almost exclusively on the understanding and quantification of the surface contribution, whereas the volume contribution has received comparatively little attention. The analysis of the anisotropy of (multi) layered systems in terms of surface and volume contributions yielded values for the latter contribution which, in general, could not be identified (straightforwardly) with known bulk values. Typical examples in this respect are the Co-based multilayers. In these systems, which are among today's most extensively studied systems, the "effective" volume magnetic anisotropy is not *a priori* evident because of the coexistence of fcc and hcp phases which differ appreciably in magnetocrystalline anisotropy, and whose formation depends sensitively on preparation conditions such as growth temperature, choice of substrate, combination of elements which are grown, etc.

In order to obtain better insight into the relation between magnetic anisotropy and structure, we began a study of a particular basic example: a thin Co film. Inevitably, such research also comprises a study of the effect of growth conditions such as, e.g., choice of substrate and growth temperature, on the crystallographic structure of the Co films. In this paper we report the results of these studies.

II. EXPERIMENT

The Co films were prepared at Philips Research Laboratories by MBE. The base pressure was 10^{-11} mbar, and the pressure during growth about 10^{-10} mbar. The deposition rate was 0.3 Å/s, and the total thickness of the films amounted to 1000 Å. Mica [001], oxidized silicon [111], and glass were used as substrates. On each type of substrate a series of samples was prepared which differed only in the substrate temperature during growth. Growth temperatures between −33 and 800 °C were used, and the films were deposited simultaneously on the different substrates. In this way for each growth temperature the effect of the substrate and for each substrate the effect of the growth temperature could be studied. For the glass substrates only temperatures up to 500 °C could be used because of the melting of the substrates at higher temperatures.

For a fast overall characterization of the sample quality, x-ray scattering was employed with the scattering vector normal to the film plane. Both θ:2θ scans and rocking scans were taken. The better quality samples were also studied on a local nanoscopic scale using nuclear magnetic resonance (NMR). The NMR experiments were performed with an incoherent spin-echo spectrometer in magnetic fields larger than the magnetic saturation field of the films, at a temperature of 1.4 K and at frequencies ranging between 180 and 195 MHz. By using a superconducting split pair magnet, fields up to 6 T could be applied at any angle with the film plane.

A vibrating sample magnetometer was used to determine the field dependence of the magnetic moment at room temperature for the magnetic field applied parallel

and perpendicular to the film plane. The accuracy in the determination of the magnetic moments was approximately 3%. From flux-gate magnetometry experiments the paramagnetic contributions to the total magnetic moment from the mica and glass substrates were found to be significant only at temperatures well below room temperature. The strength of the magnetic anisotropy was determined from the areas enclosed between the parallel and perpendicular magnetization loops.

III. CHARACTERIZATION

A. X-ray diffraction measurements

In Fig. 1 some typical results of θ:2θ scans are shown. The figure shows the (logarithmically plotted) diffracted intensity for a set of Co films grown at different temperatures T on oxidized silicon. All scans were taken *ex situ* at room temperature. As can be clearly seen from the diffraction profiles the intensity (and width) of the diffraction peaks depends on the growth temperature. For samples grown at low temperatures the profile consists of a dominant background on which some weak reflections are superimposed. These weak reflections at $2\theta \simeq 41.6°$, 47.5° and 44.4° correspond, respectively, to the (10.0) hcp, (10.1) hcp, and (111) fcc or (00.2) hcp Bragg peak. The strong broadening of the (10.1) hcp peak is characteristic of the presence of numerous extended dislocations.[2] The fact that the intensity of the peaks is comparable to the intensity of the background, as well as the mere presence of peaks of comparable intensity corresponding to different crystallographic orientations, strongly indicate a poor texture and small coherence lengths, as would be typical for a polycrystalline film.

When the growth temperature exceeds 200 °C, the Bragg peak corresponding to the (111) fcc/(00.2) hcp orientation starts to dominant the diffraction profile. Its intensity increases and is accompanied by a decrease in width. The Bragg peaks due to other crystallographic orientations remain low in intensity or disappear (for temperatures above 300 °C), indicating a longer coherence length and an improved texture of these films, i.e., an improvement of the film quality. When the growth temperature is increased above 500 °C the film quality reduces somewhat, as is evidenced by the slight decrease in intensity of the (111) fcc/(00.2) hcp Bragg peak and the development of the (200) fcc Bragg reflection at $2\theta \simeq 51.6°$.

The x-ray diffraction (XRD) profiles for films grown on glass and mica substrates are not shown here, but are comparable to those shown in Fig. 1. The films grown on glass, however, showed a strongly reduced intensity of the (111) fcc/(00.2) hcp Bragg peak and a background about four times more intense. This indicates that these films are strongly polycrystalline with a poor texture. On the contrary, the films grown on mica substrates showed an intensity of the (111) fcc/(00.2) hcp Bragg peak which was about one order of magnitude larger compared to the films on oxidized silicon, implying a far better film quality.

The variation in Bragg intensity points to significant changes in texture and coherence length as a function of the growth temperature and the substrate. Moreover, from the data in Fig. 1 also a change in position of the (111) fcc/(00.2) hcp Bragg peak as a function of the growth temperature can be observed, indicating changes

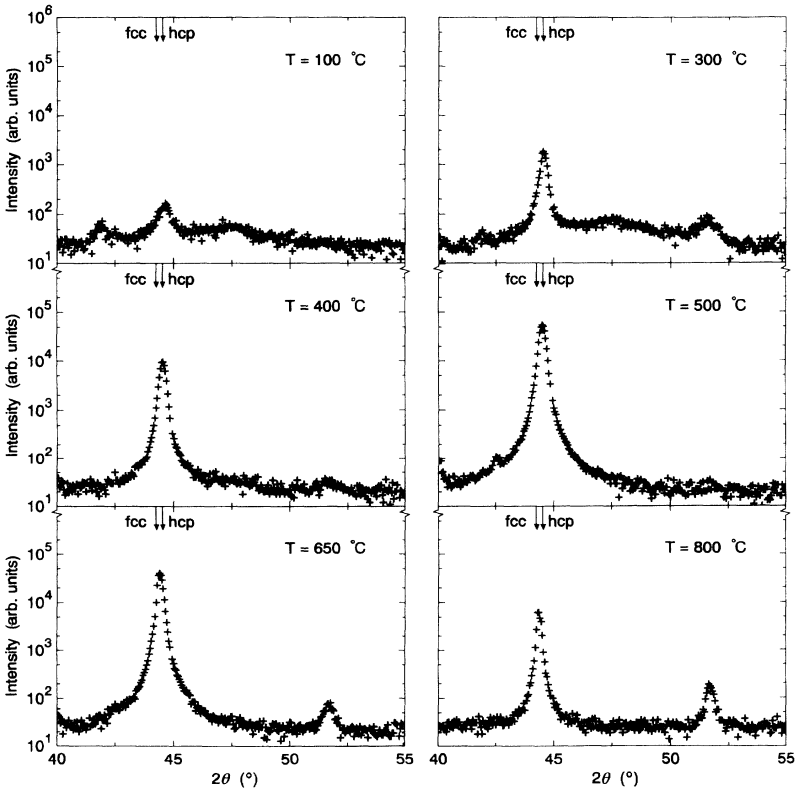

FIG. 1. Series of Cu $K\alpha$ θ:2θ scans of Co films with the scattering vector normal to the film plane as a function of the growth temperature T. The films were grown on oxidized silicon. Note that the intensities are plotted on a logarithmic scale. The main peak at $2\theta \simeq 44.4°$ corresponds to the (111) fcc–(00.2) hcp Bragg peak. The arrows denote the position of this Bragg peak in case of pure bulk fcc Co and hcp Co, respectively. The weak peaks at $2\theta \simeq 41.6°$, 47.5°, and 51.6° correspond, respectively, to the (10.0) hcp, (10.1) hcp, and (200) fcc Bragg peaks.

in the perpendicular lattice spacing. Since the lattice spacing in fcc Co along the [111] direction is slightly different from the spacing in hcp Co along the [00.2] direction, this implies changes in the structural phase composition. In order to obtain more detailed information about coherence lengths and structural phase composition, some extra θ:2θ scans of the (111) fcc/(00.2) hcp and (222) fcc/(00.4) hcp Bragg peaks were taken, and the texture of the films was probed by rocking scans of these Bragg peaks.

Texture. In Fig. 2 the full width at half maximum derived from the rocking curves is displayed as a function of the growth temperature. It is obvious that both growth temperature and choice of substrate are of significant importance for the texture of the films. The data support the conclusions obtained form the θ:2θ scans, i.e., poor texture up to 200 °C, improved texture above this temperature, and superior texture for the films grown on mica substrates. Noteworthy is that for all three types of substrate the texture improves dramatically when the growth temperature exceeds 200 °C. This seems to indicate the existence of a critical temperature below which the mobility of the Co atoms, once deposited, is too low to rearrange the atoms according to the orientation imposed by the substrate. The observed line shape of the rocking curve for the films grown on mica at 200 °C, i.e., a narrow line superimposed on a much broader one, can be considered indicative of the approach of such a critical temperature.

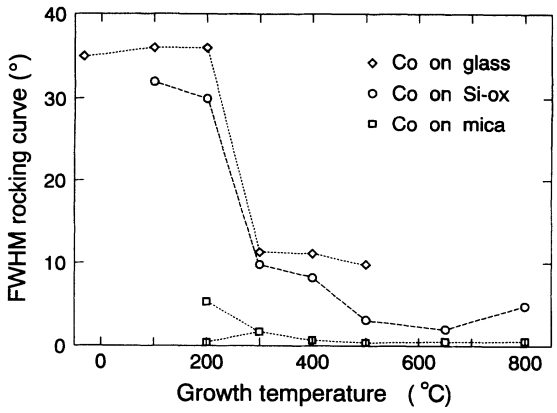

FIG. 2. Full width at half maximum of rocking curves taken at the (111) fcc–(00.2) hcp Bragg peak of Co films as a function of the growth temperature. The results reflect the texture for Co films grown on glass substrates (diamonds), oxidized silicon substrates (circles), and mica substrates (squares). The lines are guides to the eye.

Lattice spacing and coherence length. In Fig. 3 some typical results are shown of θ:2θ scans of the (222) fcc/(00.4) hcp Bragg peak. Inspection of the figure reveals that in general the diffraction peaks are composed of more than one line (the $K\alpha$ doublet is considered to be one single line of composite shape) differing in position of the peaks in the diffraction profiles is related to the per-

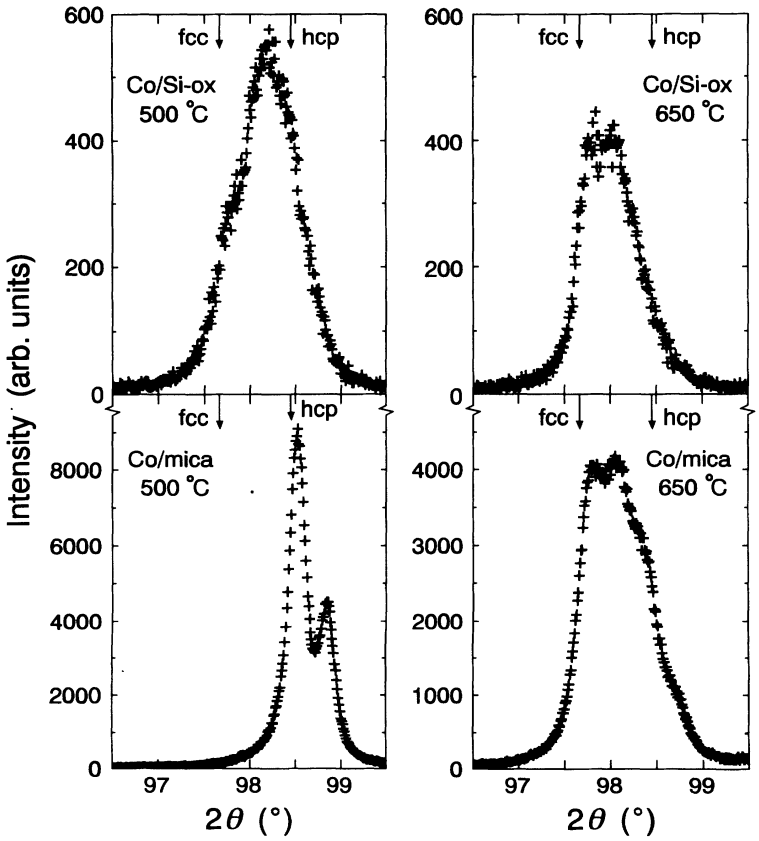

FIG. 3. Cu $K\alpha$ x-ray θ:2θ scans of Co films with the scattering vector normal to the film plane. Shown is the region around the (222) fcc–(00.4) hcp Bragg peak. The arrows denote the respective positions of the (222) fcc and (00.4) hcp Bragg peaks for pure single-phased Co. The diffraction profiles in the upper half of the figure are taken from Co films grown on oxidized silicon grown at 500 and 650 °C, respectively. The diffraction profiles in the lower half of the figure are taken from Co films grown on mica at 500 and 650 °C, respectively.

pendicular lattice spacing, and thus the structural phase, this indicates that most of the films are not single phased. The dependence of the position and relative intensities of the composing lines on growth temperature and substrate also implies a temperature- and substrate-dependent structural phase composition of the films. To quantify this the Bragg peaks were fitted using Lorentzians. For each diffraction peak the $K\alpha$ doublet was taken into account by using two Lorentzians of equal width, which were coupled in position through the wavelengths of the Cu $K\alpha 1$ and $K\alpha 2$ radiation, and in strength by their intensity ratio of 0.4. The results for the interplanar spacing and out-of-plane coherence length as obtained from the fits are shown in Figs. 4 and 5, respectively.

Figure 4 shows the results for the interplanar spacing d as a function of the growth temperature. The data were calculated from the position of the peaks using the Bragg law. The dotted lines in this figure denote the respective d spacings for the pure bulk phases. Inspection of the figure reveals that for most films more than one d spacing is observed, reflecting the mixed phase character of these films, and that the value of the d spacings depends on the growth temperature. The occurrence of Bragg peaks with a d spacing deviating from the value for bulk fcc and bulk hcp Co indicates that also numerous stacking faults are present in these films.[3] However, it is impossible to conclude from the data whether these faults correspond to hcp-like stacking faults in a fcc phase, or fcc-like stacking faults in a hcp phase, or perhaps to a combination of both. This also makes it virtually impossible to

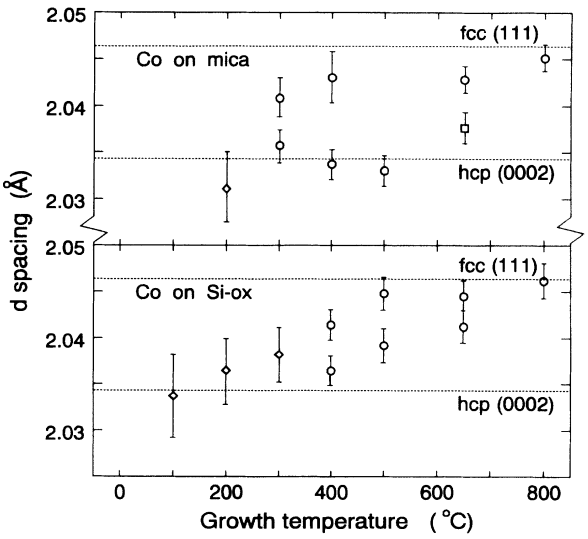

FIG. 4. Interplanar spacing as a function of the growth temperature for Co films grown on oxidized silicon and mica. The dotted lines denote the interplanar spacing for the fcc(111) and hcp(00.2) stacking for single-phased bulk Co. The data denoted by diamonds are probably not representative for the structural phase, since for these films the second-order peak was too weak to be observed and the intensity of the first-order Bragg peak was comparable to the background. The square represents an average value, since for the film grown on mica at 650 °C the corresponding part of the diffraction peak consisted of more than one line which could not accurately be resolved in the fit.

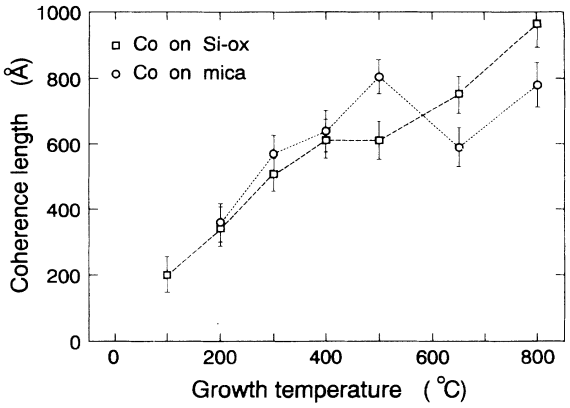

FIG. 5. Out-of-plane coherence length as a function of the growth temperature for Co films grown on mica (circles) and oxidized silicon (squares). The lines are guides to the eye.

obtain quantitative information from the measurements about the relative amounts of the fcc and hcp phases. However, the data do reveal the practically single-phased hcp character of the films grown on mica at 500 °C, and the practically single-phased character of the films grown at 850 °C.

In Fig. 5 the out-of-plane coherence length is plotted as a function of the growth temperature. The data was calculated from the width of the Bragg peaks using the Scherrer equation,[4] and is related to the out-of-plane dimensions of the crystallites as well as the number of stacking faults.[2–4] Inspection of the figure reveals an overall increase of the coherence length with growth temperature. The data also show that up to 400 °C the coherence length is almost independent of the substrate. Above this temperature the coherence length for the films on oxidized silicon continues to increase monotonically, whereas the coherence length for the films on mica shows two maxima. Since at these high growth temperatures the size of the crystallites can be expected to equal the film thickness, the data can be considered to reflect the variation in the number of stacking faults, i.e., a larger coherence length indicates a low number of stacking faults. This is supported by the fact that the films with the largest coherence length are practically single phased and have d spacings close to the bulk fcc or hcp values.

Summarizing, the x-ray diffraction data show that the film quality and the structural phase composition of Co films depend strongly on the choice of substrate and growth temperature. The films grown on mica substrates have a very good texture, and also show the most pronounced variation in structural phase composition, i.e., from almost single-phased hcp to fcc. A determination of the relative amount of each structural phase present in the films did not appear possible because of the presence of stacking faults. These cause the effective interplanar spacing to deviate from the pure bulk fcc and hcp values, making it possible to determine if it corresponds to a (faulted) fcc phase or a (faulted) hcp phase. A successful study of the relation between structure and magnetic anisotropy requires such a knowledge. Therefore we also studied these films by NMR since, as will be discussed

below, this technique allows a direct quantitative discrimination between atoms in a fcc, hcp, and stacking fault environment.

B. Nuclear-magnetic-resonance measurements

A nuclear-magnetic-resonance (NMR) experiment measures the nuclear Zeeman splitting by inducing transitions via radio-frequency electromagnetic radiation. Since this splitting is partially brought about by magnetic and electric interactions with *neighboring* ions, NMR provides, in principle, a *local* probe of the structural and magnetic properties. For a detailed discussion of the relation between the local environment and the magnetic field at the nucleus, i.e., the hyperfine field, the reader is referred to the literature.[6,7] Here it is sufficient to know that the magnitude of the hyperfine field is characteristic of the local structure, and that the anisotropy of the hyperfine field reflects the local symmetry. These features enable one to discriminate uniquely between atoms in a fcc, hcp, or stacking fault environment.

A starting point for the interpretation of the spectra is the relation

$$\Delta E = hf = \hbar\gamma |\mathbf{B}_{\rm dip} + \mathbf{B}'_{\rm hf} + \mathbf{B}_{\rm appl}| \ , \tag{1}$$

where ΔE denotes the nuclear energy level splitting, f is the NMR resonance frequency, γ is the nuclear gyromagnetic ratio ($\gamma/2\pi = 10.054$ MHz/T for ^{59}Co), $\mathbf{B}_{\rm appl}$ denotes the applied magnetic field, $\mathbf{B}_{\rm dip}$ represents the magnetic dipolar field at the nucleus resulting from all electronic Co moments, and $\mathbf{B}'_{\rm hf}$ is the hyperfine field. For the special case of the applied field parallel to the film plane, i.e., no demagnetization contribution from $\mathbf{B}_{\rm dip}$, this equation reduces to the well-known expression

$$2\pi f = \gamma(B_{\rm hf} - B_{\rm appl}) \ , \tag{2}$$

where the convention is adapted to refer to the sum of the Lorentz field and $B'_{\rm hf}$ as the actual hyperfine field $B_{\rm hf}$. The minus sign in the equation arises from the fact that in Co the hyperfine field is effectively antiparallel to the magnetic moment. Using this relation the hyperfine field $B_{\rm hf}$ can be calculated from the selected resonance frequency f and the magnitude of the applied field $B_{\rm appl}$. In principle, this gives two ways to determine the hyperfine field distribution experimentally, viz. varying the frequency at a fixed value of the applied field or sweeping the magnetic field at a fixed frequency. Here the latter method is used.

A typical example of a NMR spectrum of a Co[111] film is shown in Fig. 6. This figure shows two spectra of the same film recorded with the magnetic field applied parallel (circles) and perpendicular (squares) to the film plane, respectively. The (overall) shift between the spectra is due to the presence of the demagnetizing field for $B_{\rm appl}$ perpendicular to the film plane. Four distinct resonance lines can be distinguished. The most intense peak has a resonance field corresponding to that of bulk fcc Co, and is therefore assigned to Co atoms in the fcc phase. The signals at the high-field side of this fcc line may be attributed to both stacking faults and the hcp

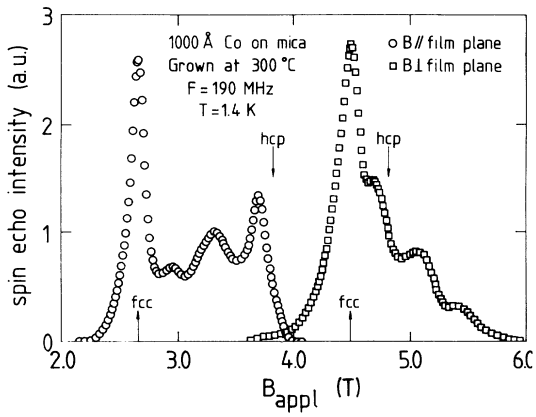

FIG. 6. NMR spectrum of a 1000-Å Co film grown on mica at 300 °C, as recorded by means of the field sweep method at a frequency of 190 MHz and a temperature of 1.4 K. Circles and squares denote the data recorded with the applied magnetic field $B_{\rm appl}$ parallel and perpendicular to the film plane, respectively. The arrows denote the resonance fields of bulk fcc and hcp Co. The overall shift in resonance field for the spectrum with $B_{\rm appl}$ perpendicular to the film plane compared to the spectrum with $B_{\rm appl}$ parallel to the film plane is caused by the demagnetization part of the dipolar field ($\mu_0 M_S \simeq 1.80$ T).

phase.[8–10] On the basis of the resonance fields (or, equivalently, $B_{\rm hf}$) alone a decisive discrimination between these phases cannot be made. However, by recording the spectrum with the field applied perpendicular as well as parallel to the film plane, use can be made of the fact that the hyperfine field of hcp Co is anisotropic by an amount of 0.86 T (at liquid-helium temperatures), whereas fcc Co and stacking faults have an isotropic (or, in the case of stacking faults, nearly isotropic) hyperfine field.[10,11] This implies that, if hcp Co is present in the sample, the corresponding resonance line in the spectra recorded with the field applied perpendicular and parallel to the film plane, respectively, will shift 0.86 T less than the (isotropic) fcc line. This is exactly what can be observed in Fig. 6 for the line at 3.7 T (field parallel). Inspection of the figure, however, also reveals that rotating the orientation of the field with respect to the film plane does not shift the complete line intensity. This is due to the existence of stacking faults with the same magnitude of the hyperfine field as hcp Co (i.e., for the field parallel to the film plane). It must therefore be stressed that care should be taken in assigning lines on the basis of the magnitude of the hyperfine (or resonance) field alone.

In the manner described above, we are able to determine which phases exist within the Co film and, since the spin-echo intensity of a line is proportional to the number of atoms in the corresponding environment, to determine the amount of Co in each phase. This provides the possibility to study the effect of manipulation of preparation conditions on the structure in a systematic way. Figure 7 contains an example of such a study. In this figure the NMR spectra for Co films grown on mica substrates at different growth temperatures are compared. As can be seen clearly from the spectra, the relative amount of the

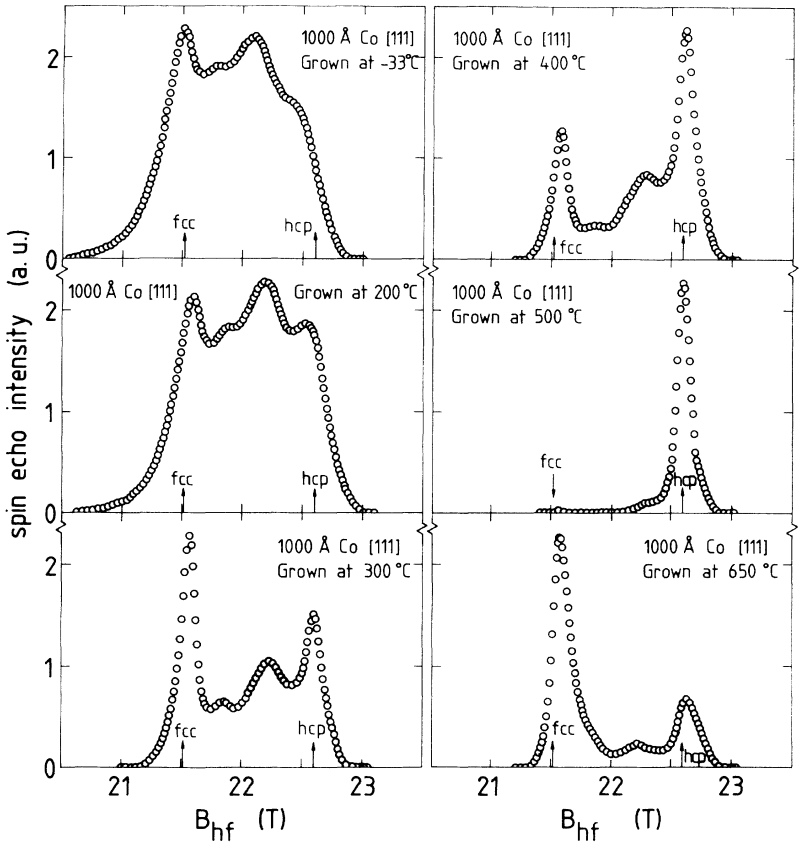

FIG. 7. NMR spectra of 1000-Å Co films grown on mica showing the variation in structure as a function of the growth temperature. The spectra were recorded at a frequency of 190 MHz, with the magnetic field applied parallel to the film plane and at a temperature of 1.4 K.

phases changes with the temperature. At low temperatures the fcc phase and stacking faults dominate. This is in fact remarkable, since for bulk Co below 425 °C hcp is the stable phase.[5] When the growth temperature exceeds 200 °C the number of stacking faults starts to decrease in favor of pure fcc and hcp phases. Note that this is also the critical temperature for the dramatic improvement in texture, as was discussed in Sec. III A. At still higher temperatures hcp becomes the stable phase, until at 500 °C almost the complete sample consists of hcp Co, as was also found by XRD. When the growth temperature is further increased, the percentage hcp phase decreases again in favor of the fcc phase and in accordance with the bulk phase transition. Figure 8 summarizes these results in a more quantitative way.

Finally we should stress that the results shown in Fig. 8 are specific for Co films grown by MBE on mica, i.e., the relative amount of the crystallographic phases and its temperature dependence is also strongly influenced for instance, by the choice of substrate, as was also indicated by the x-ray data. This is illustrated in Fig. 9. In this figure the hyperfine field spectra are compared of two 1000-Å Co films grown at 500 °C at the same time and under the same conditions but on different substrates. The Co film grown on mica shows a spectrum corresponding to almost single-phased hcp, whereas the spectrum of the film grown on oxidized silicon corresponds to that of a mixture of (about equal amounts of) fcc, hcp, and stacking faults.

The detailed knowledge of the structure of the Co films forms a good starting point for a study of the relation between the structure and the magnetic anisotropy of the electron-spin system. This topic will be discussed in Sec. IV.

IV. MAGNETIC ANISOTROPY

The magnetic saturation moment and magnetic anisotropy of each Co film were determined using a vibrating

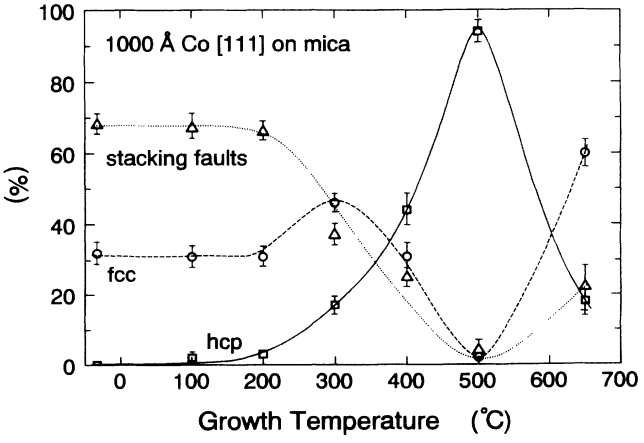

FIG. 8. Percentage of the fcc phase (circles), hcp phase (squares), and stacking faults (triangles) in 1000-Å-thick Co films grown on mica substrates as a function of the growth temperature. The results are derived from the NMR spectra in Fig. 7. The lines are guides to the eye.

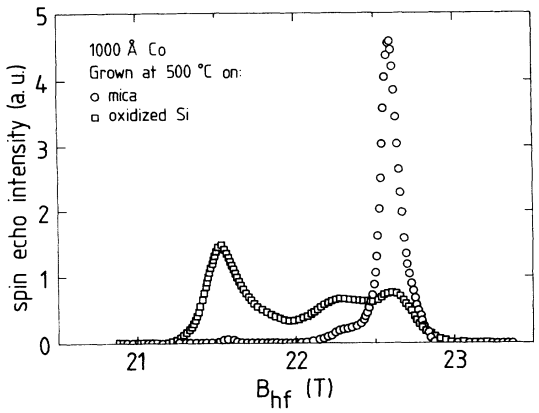

FIG. 9. NMR spectra of 1000-Å Co films grown at a temperature of 500 °C on mica (circles) and oxidized silicon (squares). The data were recorded with the magnetic field applied parallel to the film plane at a constant frequency of 190 MHz and at a temperature of 1.4 K.

sample magnetometer. Some typical results are shown in Fig. 10. This figure shows the magnetic moment as a function of the applied field at room temperature for two Co films grown on mica at temperatures of −33 and 500 °C, respectively. The film grown at −33 °C shows an almost "square" parallel loop and a linear perpendicular loop which saturates at magnetic-field strengths larger than 1300 kA/m. These features indicate a dominant in-plane anisotropy. On the other hand, the measurements

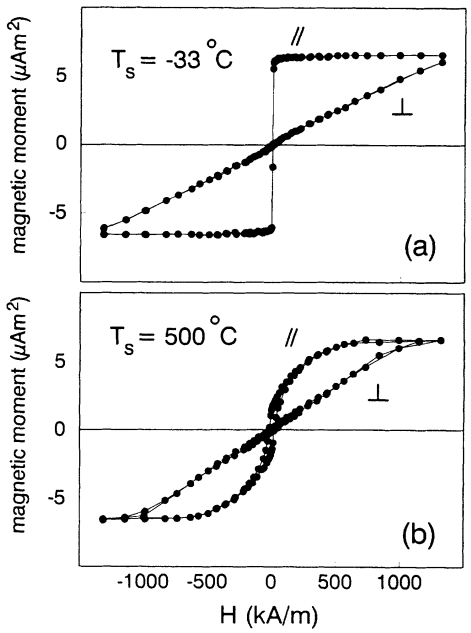

FIG. 10. Magnetic moment as a function of the applied magnetic field H for two Co films grown on mica substrates at −33 and 500 °C, respectively. The figures show the results for the magnetic field applied parallel and perpendicular to the film plane, respectively denoted by ∥ and ⊥. The loops were recorded at room temperature by means of a vibrating sample magnetometer.

on the film grown at 500 °C reveal a considerably more complex parallel loop and a perpendicular loop which saturates at lower field strengths, about 1100 kA/m. These effects are characteristic of a reduced strength of the magnetic anisotropy.

The magnitude of the magnetic anisotropy can be deduced from the measurements by the determination of the area enclosed between the parallel and perpendicular loops. The results for Co films grown on mica are shown in Fig. 11. This figure depicts the strength of the total magnetic anisotropy K_{tot} at room temperature as a function of the substrate temperature during growth. The circles denote the experimental data. The magnetic anisotropy of the films grown at low temperatures is fairly constant, and almost equals the magnetic dipolar (shape) anisotropy K_{dip} of -1.27 MJ/m^3 (for a bulk Co film with $\mu_0 M_S = 1.79$ T). However, when the growth temperature exceeds about 300 °C, the magnitude of the anisotropy rapidly decreases until, at approximately 500 °C, K_{tot} reaches a value of -0.64 MJ/m^3. Within the experimental accuracy this equals the value for a film consisting of only bulk hcp Co at room temperature [$K_{tot} = K_{dip} + K_{mc,hcp} = -0.65$ MJ/m^{3+}, where $K_{mc,hcp}$ refers to the sum of the first and second-order magnetocrystalline anisotropy constants of hcp Co (Refs. 12 and 13)]. When the growth temperature is further increased, the magnitude of K_{tot} increases again toward the value of the magnetic dipolar anisotropy.

This variation of the magnetic anisotropy between the value for bulk hcp Co and the value for pure magnetic dipolar anisotropy (which implies no hcp), suggest a relation to the presence of the hcp phase. In fact, as can be seen from a comparison of Figs. 8 and 11, the dependence of the magnetic anisotropy on the growth temperature strongly resembles the variation with growth temperature of the relative amount of hcp Co in these films. It is therefore tempting to interpret the magnetic anisotropy in terms of a simple model in which the effective total anisotropy K_{tot} is determined by the "structural phase aver-

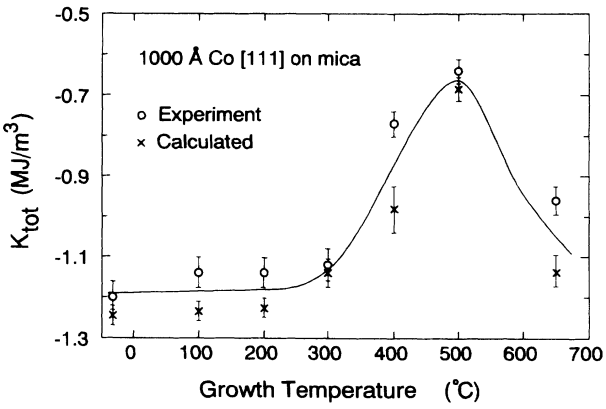

FIG. 11. Magnetic anisotropy K_{tot} at room temperature of Co films grown on mica as a function of the growth temperature. The data was obtained from VSM loops. The circles denote the experimental results, the crosses represent the calculations based on "structural phase averaging" (see text). The line is a guide to the eye.

age" over the sample:

$$K_{\text{tot}} = K_{\text{dip}} + xK_{\text{mc,hcp}} + (1-x)K_{\text{mc,fcc}} \ . \quad (3)$$

Here x represents the relative amount of the hcp phase present in the film, $K_{\text{mc,fcc}}$ denotes the magnitude of the magnetocrystalline anisotropy of bulk fcc Co, and $K_{\text{mc,hcp}}$ and K_{dip} have already been discussed. For practical purposes the last term on the right-hand side in Eq. (3) may be neglected, since $K_{\text{mc,fcc}}$ is practically zero.[14] Within the model stacking faults are treated on the same footing as the fcc phase. An indication that this is justified follows from the NMR measurements, which reveal that for Co atoms within a stacking fault the resonance frequencies or, equivalently, B_{hf}, have an angular dependence similar to the fcc Co line.

The crosses in Fig. 11 denote the results of a calculation based on Eq. (3) and the experimentally determined amounts of the different phases as shown Fig. 8, assuming bulk Co room-temperature values for the magnetocrystalline and dipolar anisotropies. It is obvious that the qualitative behavior of the magnetic anisotropy is well reproduced and, in view of the simplicity of the model, the agreement between experimental and calculated data is rather good.

The results discussed above indicate that on a macroscopic level the overall anisotropy of the Co films can be described to a reasonable degree of accuracy by a simple average over the various volume fractions. Physically such an average will be obtained both when the electron spins are strongly exchange coupled and when they are virtually uncoupled as, e.g., might occur in a film consisting of separate crystallites of hcp Co and fcc Co. If the film consists of uncoupled crystallites of two different structural phases, the saturation field is different for these two phases, and the perpendicular magnetization loop would be expected to show a linear increase of the magnetic moment, which changes slope at the saturation field of the hcp phase. As can be seen from a comparison of Figs. 10(a) and 10(b), the introduction of hcp Co at higher growth temperatures indeed yields more complicated $M(H)$ curves which might reflect separate contributions from fcc and hcp magnetization fractions. However, the available magnetization data do not permit detailed analysis and conclusions about the coupling of the magnetic moments.

An alternate approach is the determination of the "local" anisotropy, i.e., within each individual phase, as can be obtained by NMR. The behavior of the hyperfine field is related to the behavior of the electronic magnetic moment (B_{hf} is antiparallel to the magnetic moment) and, moreover, it can be probed individually for the fcc and hcp phases because their respective hyperfine fields are different. Actually, the determination of the total anisotropy by NMR is based on the fact that, due to the presence of magnetic anisotropy, the magnetic moment (and therefore also the hyperfine field) is retarded with respect to the external field when an external field is applied at an angle with the film plane. Because NMR effectively measures the vector sum of external and hyperfine fields [cf. Eq. (1)], the retardation of the hyperfine field manifests itself in the (angular dependence of the) resonance frequency (or, equivalently, the resonance field).

Table I contains the local magnetic anisotropies $K_{\text{loc,NMR}}$ at 1.4 K as determined from such data for the Co films grown on mica at 400 and 500 °C. For comparison in the table the bulk anisotropy values at 1.4 K, $K_{\text{tot,bulk}}$, and the anisotropies $K_{\text{tot,cal}}$ as calculated from Eq. (3), are also included. Inspection of the table reveals that on an atomic scale the magnetic anisotropies differ from the bulk single-phase values, and that this difference depends on the ratio between the amounts of hcp and fcc in the films. This evidences the strong coupling between the moments of the various structural phases and, therefore, indicates that the multiple-phase character of the films arises from growth faults within the crystallites rather than from the combined presence of single-phased fcc and hcp crystallites. The variation in local anisotropy for the different phases also shows that on a nanoscopic level the concept of one single average anisotropy is somewhat oversimplified.

V. CONCLUDING REMARKS

Using x-ray diffraction and nuclear magnetic resonance the effect of substrate and growth temperature on the quality and structural phase composition of 1000-Å-thick Co films was studied. For growth temperatures up to 200 °C the films show, almost independent of the type of substrate, a state of strong polycrystallinity with a

TABLE I. Local anisotropy $K_{\text{loc,NMR}}$ at a temperature of 1.4 K for the fcc and hcp phases in [111]/[00.2] 1000-Å Co films grown on mica substrates at 400 and 500 °C as derived from the NMR measurements. $K_{\text{loc,}}$NMR is obtained from fits to the equilibrium condition for the local electron-spin moment of the angle between the hyperfine field at resonance (i.e., the local magnetic moment of the electron-spin system) and the applied magnetic field for various out-of-plane directions of the applied field. $K_{\text{loc,NMR}}$ must be compared with the total magnetic anisotropy $K_{\text{tot,bulk}}$ at 1.4 K of bulk fcc and hcp Co, respectively, which is defined as the sum of first- and second-order bulk anisotropy constants including the magnetic dipolar anisotropy of -1.27 MJ/m^3. $K_{\text{tot,cal}}$ represents the total anisotropy as calculated from Eq. (3) using the values for $K_{\text{mc,hcp}}$ at 1.4 K and the results displayed in Fig. 7 (see text). All anisotropy values are in units of MJ/m^3.

	fcc		hcp		
Sample	$K_{\text{loc,NMR}}$	$K_{\text{tot,bulk}}$	$K_{\text{loc,NMR}}$	$K_{\text{tot,bulk}}$	$K_{\text{tot,cal}}$
Co on mica (400 °C)	-1.12 ± 0.04	-1.27	-0.84 ± 0.15	-0.42	-0.90
Co on mica (500 °C)	-0.90 ± 0.06	-1.27	-0.45 ± 0.09	-0.42	-0.47

moderate texture. Above this temperature the texture strongly improves and the number of stacking faults in the films decreases. The best film quality is obtained for mica substrates and a growth temperature between 400 and 500 °C.

The structural phase composition of the films appeared to be strongly dependent on growth temperature as well as on the type of substrate, and was different from that expected from the bulk phase transition. This supports the experimental observations that in multilayers the actually realized structure is determined by the choice of base layer and nonmagnetic intermediate layers rather than by the bulk phase transition.[15–18] The experiments also reveal that with NMR unique quantitative and qualitative information on the local nanoscopic structural phase can be obtained; more specifically, it is very easy to discriminate between fcc, hcp, and stacking faults. As such in a structural analysis NMR forms a valuable complement to, e.g., x-ray diffraction and TEM.

Using the structural information obtained from NMR and XRD, the relation between the overall magnetic anisotropy and the structural phase composition was studied. It appears that the magnetic anisotropy reflects the structural phase composition of the films. The magnitude of the magnetic anisotropy could be well described by a simple model based on a compositional averaging of the bulk anisotropies. The local anisotropy for each separate phase was determined from the NMR measurements, and indicated a strong coupling between the magnetic moments of the atoms in the fcc and hcp phases. The variation of the local anisotropy within the film also shows that on a nanoscopic level the concept of one single average anisotropy is somewhat oversimplifed.

ACKNOWLEDGMENTS

We are indebted to W. Hoving at the Philips Research Laboratories in Eindhoven for the preparation of the samples, to Dr. K. Kopinga for the stimulating discussions, and to A. van Steenbergen for the experimental assistance. The research forms part of a joined effort of Eindhoven University of Technology and Philips Research Laboratories on the area of magnetic multilayers. Part of the research was sponsored by the EEC in SCIENCE Project GP^2M^3.

---

*Present address: Institut für Feskörperforschung, Forschungszentrum Jülich, P.O. Box 1913, D-52425 Jülich, Germany.

[1]For a recent review on this subject see, e.g., W. J. M. de Jonge, P. J. H. Bloemen, and F. J. A. den Broeder, in *Ultrathin Magnetic Structures,* edited by B. Heinrich and J. A. C. Bland (Springer-Verlag, Berlin, in press).

[2]C. R. Houska and B. L. Averbach, Acta Crystallogr. **11**, 139 (1958); C. R. Houska, B. L. Averbach, and M. Cohen, Acta Metall. **8**, 81 (1960).

[3]M. S. Paterson, J. Appl. Phys. **23**, 805 (1952); M. T. Sebastian and P. Krishna, Phys. Status Solidi A **101**, 329 (1987).

[4]Any textbook on x-ray diffraction, e.g., D. B. Cullity, *Elements of X-Ray Diffraction* (Addison-Wesley, London, 1978).

[5]M. Hansen, *Constitution of Binary Alloys* (McGraw-Hill, New York, 1958).

[6]H. Akai, M. Akai, S. Blügel, B. Drittler, H. Ebert, K. Terakura, R. Zeller, and P. H. Dederichs, Prog. Theor. Phys. **101**, 11 (1990).

[7]H. A. M. de Gronckel and W. J. M. de Jonge, in *Magnetic Multilayers,* edited by L. H. Bennett and R. E. Watson (World Scientific, New Jersey, in press).

[8]L. E. Toth and S. F. Ravitz, J. Phys. Chem. Solids **24**, 1203 (1963).

[9]H. Brömer and H. L. Huber, J. Magn. Magn. Mater. **8**, 61 (1978).

[10]M. Kawakami, T. Hihara, Y. Koi, and T. Wakiyama, J. Phys. Soc. Jpn. **33**, 1591 (1972).

[11]D. Fekete, H. Boasson, A. Grayevski, V. Zevin, and N. Kaplan, Phys. Rev. B **17**, 347 (1978).

[12]F. Ono, J. Phys. Soc. Jpn. **50**, 2564 (1981).

[13]W. Sucksmith and J. E. Thompson, Proc. R. Soc. London Ser. A **225**, 362 (1954).

[14]D. S. Rodbell, J. Phys. Soc. Jpn. **17**, 313 (1962).

[15]C. M. Schneider, J. J. Miguel, P. Schuster, and R. Miranda, in *Science and Technology of Nanostructured Magnetic Materials* (Plenum, New York, 1991), p. 37.

[16]H. A. M. de Gronckel, J. A. M. Biernet, F. J. A. den Broeder, and W. J. M. de Jonge, J. Magn. Magn. Mater. **93**, 457 (1991).

[17]P. Boher, F. Giron, Ph. Houdy, F. Baudelet, A. Fontaine, J. M. Ladouceur, E. Dartyge, P. Beauvillain, C. Chappert, P. Veillet, and K. LeDang, J. Appl. Phys. **71**, 1798 (1992).

[18]C. Mény, P. Panissod, and R. Loloee, Phys. Rev. B **45**, 12 269 (1992).